Chapitre 3

Variable Admittance for pHRI : from Intuitive Unilateral Interaction to Optimal Bilateral Force Amplification

Résumé

Dans cet article, une nouvelle architecture de commande pour les manipulateurs robotisés à plusieurs degrés de liberté (multi-ddls) utilisés dans un contexte d'interaction physique humain-robot (pHRI) est présentée. Un régulateur en admittance est utilisé comme structure de commande unique pour les différents modes d'interaction. Cette approche est reconnue pour la manipulation intuitive qui en résulte lors d'interactions unilatérales. Cependant, l'efficacité de ce type de commande pour les amplifications bilatérales sur des environnements rigides est souvent questionnée. Ici, des paramètres d'admittance variables sont utilisés afin d'adapter et d'optimiser la réponse du système pour toutes les dynamiques potentielles du manipulateur. Trois lois de commande variables interdépendantes sont alors présentées, à savoir, une commande unilatérale par admittance variable standard, une commande bilatérale par admittance à séquencement de gain et une commande transitionnelle continue. Un manipulateur Kuka LWR 4 à sept degrés de liberté est utilisé pour l'expérimentation et pour la démonstration de l'efficacité des algorithmes de commande. Une vidéo montrant différentes tâches de pHRI utilisant l'architecture de commande proposée est aussi fournie.

3.1 Introduction

In a previous work (Labrecque and Gosselin [2014]), the authors demonstrated the performance and the stability of a single-dof force amplification controller based on the admittance model presented in Lecours et al. [2012]. The key feature of this simple architecture is its ability to vary its parameters, which leads to a more intuitive interaction, higher performances, and

a smooth transition between the unilateral free space motion and the bilateral constrained mode.

In this chapter, an optimal multi-dof version of the pHRI controller presented in Labrecque and Gosselin [2014] using variable admittance regulators is proposed. Human dynamics, multiple modes of interaction and varying robot configurations introduce significant control challenges in terms of the performance and stability of the system. Such challenges are typically addressed using a single static controller which can be tuned to ensure stability but at the expense of performance. Alternatively, different controller structures can be used for each interaction mode in order to increase the performance. However, this approach increases complexity and can make it difficult to guarantee that the transitions between controller structures are always stable. In this chapter, it is demonstrated that a single control structure with varying parameters can result in an intuitive and optimal response for all types of interactions. Section 3.2 discusses the interaction interface and presents the general inner and outer control loops of the proposed controller structure. Then, Section 3.3 describes the variable admittance control law and its stability for unilateral interactions, followed by the optimal gain scheduling control law in Section 3.4 for bilateral interactions. The continuous transition control law is then presented in Section 3.5 for the smooth mode switching. Section 3.6 demonstrates the effectiveness of the control algorithms using three experiments. A complementary video is provided and described in Section 3.7. Finally, conclusions are presented in the last section. For the rest of the thesis, the term unilateral interaction refers to the mode in which the robot end-effector is able to move in free space with the help of one or many physical human interactions. By contrast, for a bilateral interaction, the human interaction guides the robot end-effector to apply a force to an external environment.

3.2 General control architecture

3.2.1 Interaction Interface

Cooperative force amplification implies a direct contact between the robot and the human operator and between the robot and the environment, and thus force sensors are required to measure the operator input and the environment output. For a single-dof manipulator, since there is only one moving link, both sensors are mounted at the effector (the moving link). Although having both sensors at the end-effector of a multi-dof robot has numerous advantages, this arrangement becomes less relevant for the present study. Indeed, one of the many goals of introducing human-robot cooperation in industry is to alleviate musculoskeletal problems by reducing the effort of repetitive and uncomfortable tasks. Positioning both sensors at the end-effector of the robot would allow perfect task-motion transparency, but it would also regrettably preserve the resulting arduous postures of the human operator. It is therefore desirable to mount the operator input sensor on a different manipulator link. In this work, a

7-dof redundant serial manipulator is used. A way to achieve an intuitive physical interaction for a 7-dof serial robot including a spherical wrist, is to locate the operator sensor on the fourth link. If the inverse kinematics resolution — redundancy resolution in this case — is resolved at the centre of the spherical wrist a rotational motion of the end-effector would not affect the operator sensor. This choice of location leads to theoretically pure translational motions and thereby eliminates the discomfort induced by rotational motions. It should be pointed out that the control architecture proposed in this work does not require the use of a redundant robot and that this discussion on the location of the force sensors also applies to 6-dof robots. Another option that renders an intuitive interaction is using the operator physical input directly on the manipulator's links. This is possible if torque sensors are available at each of the robot joints. In this chapter, an external six-axis force/torque sensor mounted on the fourth link of the robot and seven joint torque sensors are combined. This combination leads to the best interaction without compromising the amplification, as further explained in subsection 3.2.3 and section 3.4.

As stated in the introduction, admittance control is widely used for unilateral pHRI because of the direct relationship between its parameters and the dynamics felt by the operator as well as the resulting intuitive and stable interaction. However, admittance control is often disregarded for bilateral interactions (or for contacts with rigid environments) and is quickly replaced by impedance control (Ott et al. [2010]) or even direct force control (Lamy et al. [2009]). This decision is mainly driven by the fact that the relationship with a desired virtual dynamics is lost. A regulator with a force output would thus seem more appropriate. However, a unilateral or bilateral interaction with a human operator or a rigid surface leads to a wide range of different dynamics to regulate. A single static controller is thus rarely adequate. Moreover, when two different controllers are used, an efficient switching law has to be implemented (Shaikh and Caines [2007]) in order to avoid the flickering effect. On the other hand, a single controller with variable parameters can adapt to different interaction modes as demonstrated in Pitakwatchara et al. [2006] using a discrete control law for teleoperation and in Labrecque and Gosselin [2014] using a continuous control law for a single-dof force amplification system.

The potential benefits of using a variable admittance for bilateral interactions with different environments have been demonstrated in Labrecque and Gosselin [2015] for a multi-dof manipulator, namely, the Kuka LWR. Therefore, in this chapter, the continuous control law presented in Labrecque and Gosselin [2014] and the optimal force amplification scheme from Labrecque and Gosselin [2015] are unified in order to obtain an intuitive and versatile pHRI for a multi-dof manipulator that uses a single controller. The proposed architecture is shown in Fig. 3.1.

The control architecture includes two main loops, namely, an inner loop for the precise positioning and an outer loop for the transformation of the different interaction forces into desired motions. The components of the controller are detailed in the following subsections.

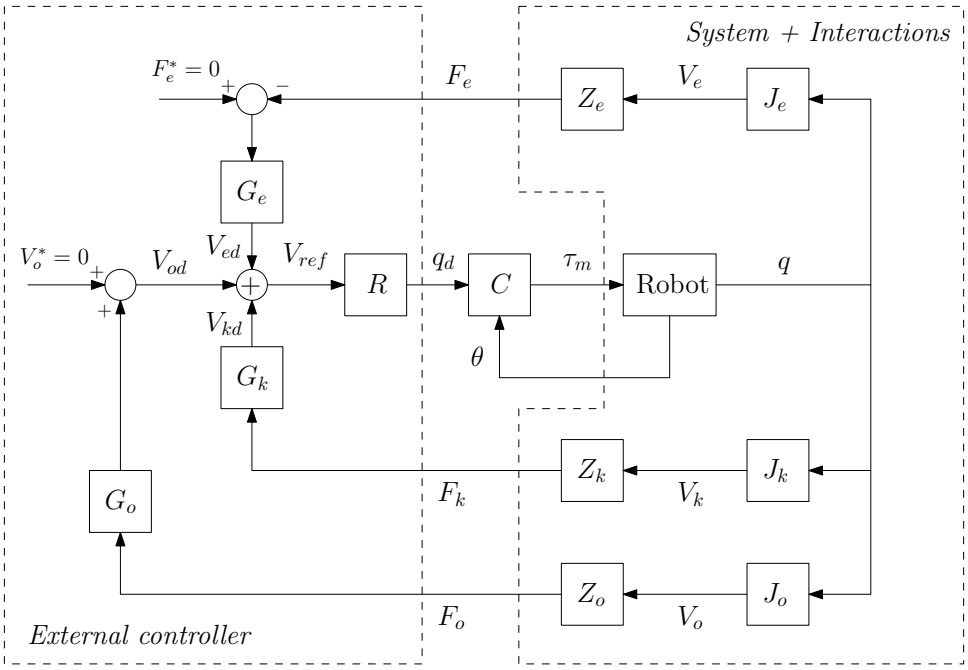

FIGURE 3.1 – General admittance control architecture proposed for a pHRI using a multi-dof manipulator. In order to not surcharged the schematic, torques generated by the external forces are excluded.

3.2.2 Inner position control

The inner controller of the proposed architecture, noted C in Fig. 3.1, of the proposed architecture can be a simple PD controller on the position command. However, since the manipulator used for the experimentation in this work is a Kuka LWR 4, the internal position control of the Kuka was selected.

The Kuka LWR is defined as a flexible manipulator and has, therefore, a particular controller in order to take into consideration the elasticity of its joints. The controller is described in Albu-Schäffer et al. [2007] and Ott et al. [2008], and hence, it is only briefly summarized in this section.

A robot with rigid links and flexible joints can be assumed to have the following dynamic model :

$$\mathbf{M}(\mathbf{q})\ddot{\mathbf{q}} + \mathbf{C}(\mathbf{q}, \dot{\mathbf{q}})\dot{\mathbf{q}} + \mathbf{g}(\mathbf{q}) = \mathbf{K}(\boldsymbol{\theta} - \mathbf{q}) - \boldsymbol{\tau}_{ext}, \tag{3.1}$$

$$\mathbf{B}\ddot{\boldsymbol{\theta}} + \mathbf{K}(\boldsymbol{\theta} - \mathbf{q}) = \boldsymbol{\tau}_m \tag{3.2}$$

where $\mathbf{M}(\mathbf{q})$, $\mathbf{C}(\mathbf{q}, \dot{\mathbf{q}})$, and $\mathbf{g}(\mathbf{q})$ are respectively the link inertia matrix, the centripetal and Coriolis vector, and the gravity vector. $\mathbf{B}$ is the diagonal actuator inertia matrix and $\mathbf{K}$ is the diagonal joint stiffness matrix. Vectors $\boldsymbol{\theta}$ and $\mathbf{q}$ are respectively the joint position vector associated with the actuators and the joint position vector associated with the links. $\boldsymbol{\tau}_{ext}$ is the external torque vector and includes the two force inputs from the operator and the

environment force input. In order to avoid overloading the schematic, the components of $\boldsymbol{\tau}_{ext}$ are not shown in Fig. 3.1. Finally, $\boldsymbol{\tau}_m$ is the actuator torque vector.

It is thus possible to define the following position control law

$$\boldsymbol{\tau}_m = -\mathbf{K}_P(\boldsymbol{\theta} - \boldsymbol{\theta}_d) - \mathbf{K}_D\dot{\boldsymbol{\theta}} + \mathbf{K}_T(\mathbf{g}(\mathbf{q}) - \boldsymbol{\tau}) + \mathbf{g}(\mathbf{q}) \tag{3.3}$$

where $\mathbf{K}_P$, $\mathbf{K}_D$, and $\mathbf{K}_T$ are the gain matrices which are defined as positive definite diagonal matrices, where the joint torque vector $\boldsymbol{\tau}$ is defined by

$$\boldsymbol{\tau} = \mathbf{K}(\boldsymbol{\theta} - \mathbf{q}), \tag{3.4}$$

and where the desired actuator position vector $\boldsymbol{\theta}_d$ is defined with the gravity vector $\mathbf{g}(\mathbf{q}_d)$ and the desired link position vector $\mathbf{q}_d$, and yields

$$\boldsymbol{\theta}_d = \mathbf{q}_d + \mathbf{K}^{-1}\mathbf{g}(\mathbf{q}_d). \tag{3.5}$$

3.2.3 Outer force to velocity control : admittance

The external controller is a summation of the different Cartesian interaction forces which are beforehand processed by admittance regulators. An admittance regulator transforms an input force into a motion command. Hence the external controller is a summation of the different Cartesian velocity commands generated by the input forces. Typically, for a single Cartesian dof, the relationship is of the form

$$f = m(\ddot{x} - \ddot{x}_t) + c(\dot{x} - \dot{x}_t) + k(x - x_t) \tag{3.6}$$

where f is the external force, m, c, and k are respectively the virtual inertia, damping and stiffness, $\ddot{x}$, $\dot{x}$, and x are the Cartesian acceleration, velocity, and position, and finally, $\ddot{x}_t$, $\dot{x}_t$, and x_t represent the desired trajectory to be followed. Since the input is coming from a physical interaction, $\ddot{x}_t$, $\dot{x}_t$, and x_t should be set to zero. The virtual stiffness, k, should also be equal to zero in order to obtain a free motion. The relationship is then rewritten as follows

$$f = m\ddot{x} + c\dot{x}. \tag{3.7}$$

It is then easy to solve the above equation for the velocity in the Laplace domain, yielding

$$\dot{X}(s) = \frac{1}{ms + c}F(s) = \frac{\frac{1}{c}}{\frac{m}{c}s + 1}F(s) = Y(s)F(s) \tag{3.8}$$

where $\dot{X}(s)$ and $F(s)$ are respectively the Laplace transforms of $\dot{x}$ and f, $Y(s)$ is the admittance, and s is the Laplace variable.

Each admittance regulator is combined with an amplification factor in order to yield priorities to a specific interface during unilateral interactions or to adjust the amplification ratio during bilateral interactions. The general external regulator matrix thus yields

$$\mathbf{G}_x = \boldsymbol{\beta}_x\mathbf{Y}_x \tag{3.9}$$

where $\boldsymbol{\beta}_x$ is the diagonal amplification factor matrix and $\mathbf{Y}_x$ is the diagonal admittance matrix.

In the control architecture of Fig. 3.1, three interaction dynamics matrices are involved. From Fig. 2.6, these potential input dynamics are the Cartesian operator impedances acting on the six-axis force/torque sensor located at the fourth manipulator link, noted $\mathbf{Z}_o$, the Cartesian operator impedances acting on the internal torque sensors, noted $\mathbf{Z}_k$, and the Cartesian environment impedances acting on the six-axis force/torque sensor located at the end-effector, noted $\mathbf{Z}_e$. These dynamics can produce three input force vectors which are, respectively, $\mathbf{F}_o$, $\mathbf{F}_k$, and $\mathbf{F}_e$. Each input force vector is passed through an external regulator matrix, $\mathbf{G}_o$, $\mathbf{G}_k$, or $\mathbf{G}_e$ which includes an amplification factor matrix, $\boldsymbol{\beta}_o$, $\boldsymbol{\beta}_k$, or $\boldsymbol{\beta}_e$, and an admittance regulator matrix, $\mathbf{Y}_o$, $\mathbf{Y}_k$, or $\mathbf{Y}_e$.

The desired velocity vectors, $\mathbf{V}_{od}$, $\mathbf{V}_{kd}$, and $\mathbf{V}_{ed}$, which are computed from the input force vectors, are added up to give the reference velocity vector $\mathbf{V}_{ref}$. For a single degree of freedom, the resulting reference velocity is expressed as follows :

$$v_{ref} = \beta_o y_o f_o + \beta_k y_k f_k + \beta_e y_e f_e. \tag{3.10}$$

In order to avoid a misinterpretation of the measured forces, when an environment force f_e is sensed at the end-effector, the amplification factor β_k associated with the internal joint force sensors is set to zero[1]. Moreover, if the controlled manipulator is in steady state during a bilateral interaction, then the desired joint position q_d should be constant and the reference velocity v_{ref} should thus be equal to zero. Equation (3.10) then yields

$$0 = \beta_o y_o f_o + \beta_e y_e f_e \tag{3.11}$$

with similar admittance parameters in y_o and y_e, which therefore leads to

$$f_o = -\frac{\beta_e}{\beta_o} f_e. \tag{3.12}$$

The operator and environment forces are thus, logically, in opposite directions and proportional with an amplification ratio of β_e/β_o, which is the desired controller behaviour.

Finally, the redundancy resolution, R in Fig. 3.1, which tranforms the Cartesian reference velocities into seven joint positions, is carefully chosen in order to render the most intuitive interaction possible. Indeed, a 7-dof manipulator can react non-intuitively to a physical human interaction. It can be caused by a singularity or by a specific resolution chosen. The typical resolution uses the Moore-Penrose generalized inverse matrix which yields the minimum norm solution. Unfortunately, a human operator can easily push the robot into a singular configuration which may yield an uncontrollable situation. A common method to avoid this issue is to add a damping factor in the resolution, as proposed by Wampler [1986] based on the Levenberg-Marquardt method (Marquardt [1963]). This technique prevents the robot from

1. The forces and torques applied at the end-effector have a direct impact in the joint torques

reaching a singular configuration but can also lead to a counter-intuitive slow-down when approaching a singularity. In order to eliminate these numerical singularities, Sugihara proposed a simple solution by using the squared norm of the residual for the damping factor (Chan and Lawrence [1988]), but with a small added bias (Sugihara [2011]). The corresponding equation to resolve the redundancy with a velocity input, $\mathbf{v}_{ref}$, and a position output, $\mathbf{q}_d$, is written as follows

$$\mathbf{q}_{d[i+1]} = \mathbf{q}_{d[i]} + \mathbf{W}_J \mathbf{J}^T (\mathbf{J}\mathbf{W}_J \mathbf{J}^T + \mathbf{W}_N)^{-1} \mathbf{e} \tag{3.13}$$

where $\mathbf{J}$ is the Jacobian matrix, $\mathbf{W}_J$ is a $[7 \times 7]$ weighting matrix, $\mathbf{W}_N$ is the damping factor and yields

$$\mathbf{W}_N = E\ \mathbf{I}_{[6\times6]} + w_N \mathbf{I}_{[6\times6]} \tag{3.14}$$

with w_N being the added small bias — in this work $w_N = 0.01$ — and with E being the squared norm

$$E = \frac{1}{2} \mathbf{e}^T \mathbf{W}_E \mathbf{e} \tag{3.15}$$

of the residual

$$\mathbf{e} = \mathbf{v}_{ref} T_s. \tag{3.16}$$

The residual is simply the reference velocity multiplied with the sampling time T_s which gives the distance between the actual position and the desired position for a single time step. The matrix $\mathbf{W}_E$ is a $[6 \times 6]$ weighting matrix. This method ensures the numerical convergence of the resolution for any input motion and is therefore used in the control architecture proposed in this chapter.

The control architecture presented is the general framework of the controlled manipulator. Indeed, in order to accommodate the different interactions it is necessary to define specific control laws for each mode. These control laws involve varying parameters and are described in the next section.

3.3 Unilateral mode

The use of the term unilateral interaction might be perceived as slightly inadequate in this chapter because of the two different means to sense the operator force input, namely, the six-axis force/torque sensor on one of the robot links and the internal joint force sensors. However, even if the operator can simultaneously use his two hands in two different locations on the manipulator, it is important to make a distinction between the interactions intended for a free motion of the end-effector (unilateral interactions) and the interactions intended for a contact of the end-effector with a rigid surface (bilateral interactions). In this section the control and stability of the unilateral mode is thus detailed.

3.3.1 Control law

When the end-effector is free to move, only the force sensor mounted on the fourth link and the joint torque sensors are active. In this mode, the controller yields a typical first order admittance dynamics. This system, based on equation (3.8), has a well-known behaviour in the time domain. It is therefore easy to infer the effect of the two parameters on the system response, namely, the inverse of the virtual damping which acts as a DC gain and the ratio of the virtual inertia over the virtual damping which acts as a time constant. The resulting dynamics, when applying an external force, can also be considered as that of a mass, m, moving in a viscous environment of damping coefficient, c. Therefore, if the admittance parameters are high then the robot will be less reactive to the sensed force. On the other hand, if they are low it will be easier to move the robot, but more difficult to control it for precise motion. In fact, it has been shown that the most intuitive pHRI can be obtained by varying the admittance parameters online according to the operator's intentions (Lecours et al. [2012], Duchaine and Gosselin [2007], Tsumugiwa et al. [2001]). The approach proposed in Lecours et al. [2012] is used here for the diagonal components of the human admittance regulator matrices, $\mathbf{Y}_o$ and $\mathbf{Y}_k$. It is briefly recalled in the following for a single dof system.

In this approach, the effective damping coefficient, noted c_{ov}, is calculated based on the nominal (default) damping coefficient, c_o, and the desired acceleration, $\ddot{x}_d$, using

$$c_{ov} = \begin{cases} c_o - \alpha|\ddot{x}_d| & \text{for acceleration} \quad (3.17) \\ c_o + \alpha|\ddot{x}_d| & \text{for deceleration} \quad (3.18) \end{cases}$$

where parameter α is used to adjust the influence of the acceleration, or deceleration, on the variation of c_{ov}.

When it is desired to accelerate, the virtual damping decreases and the effective virtual inertia, noted m_{ov}, is adjusted in order to keep a constant ratio of damping over inertia. This variation leads to a more reactive interaction for larger accelerations. However, when it is desired to decelerate, the virtual damping increases, and the virtual inertia partially decreases, which leads to a more precise positioning. The following relations are used to adjust the virtual inertia

$$m_{ov} = \begin{cases} \dfrac{m_o c_{ov}}{c_o} & \text{for accel} \quad (3.19) \\ \dfrac{m_o c_{ov}}{c_o}(1 - \eta(1 - e^{\gamma(c_o - c_{ov})})) & \text{for decel} \quad (3.20) \end{cases}$$

where m_o is the nominal virtual inertia and η and γ are parameters that are used to respectively adjust the steady state inertia over damping ratio and the rate of the transition. In the above, the desired acceleration, $\ddot{x}_d$, is computed using a discrete form of (3.7).

It is important to mention that the admittance parameters are similar for $\mathbf{Y}_o$ and $\mathbf{Y}_k$, but that the components of the amplification factor matrices, $\boldsymbol{\beta}_o$ and $\boldsymbol{\beta}_k$, can take different values

in order to prioritize a certain interaction or certain Cartesian motions. In this work, it is expected that the operator will mostly interact with the handle mounted on the fourth link. Interactions sensed on the six-dof force/torque sensor of the handle are therefore given priority.

3.3.2 Stability and performance

For pHRI, preliminary stability assessment can be done before experimentation. However, because of the varying dynamics and notion of comfort specific to human beings, it is almost always necessary to reassess the stability boundaries based on a human feedback. A pHRI study using a Kuka LWR 4 with a similar varying admittance controller for unilateral interactions (Ficuciello et al. [2014]) has experimentally evaluated the boundaries of the virtual parameters, c_{ov} and m_{ov}. In order to obtain stable interactions, the boundaries proposed in Ficuciello et al. [2014] have thus been used in this chapter for the unilateral mode. The performance preferences differ from one operator to the other and can be adjusted individually or kept to a common average.

3.4 Bilateral mode

3.4.1 Control law

When the end-effector comes into contact with the environment, the force sensor at the end-effector becomes active and the bilateral mode is enabled. The control architecture is unchanged but the admittance parameters are modified in order to take into consideration the new interaction dynamics. Indeed, a rigid surface has a highly reactive dynamics and can easily compromise the coupled stability and performance of a bilateral system. In order to obtain a stable amplification, the regulator's DC gains and time constants have to be low, and equation (3.12) has to be satisfied. This means that the admittance parameters of $\mathbf{Y}_o$ and $\mathbf{Y}_e$ have to be similar and that the amplification factors of $\boldsymbol{\beta}_k$ have to be equal to zero. Indeed, if the interactions with the joint torque sensors are kept in the control loop, then the environment forces will be numerically cancelled because of the sensor redundancy. A stable amplification will therefore be impossible.

The smooth transition to go from a mode to another is detailed in the next section. However, another important control issue appears with the use of a multi-dof manipulator for bilateral amplification. Indeed, the dynamics of a multi-dof manipulator is configuration dependent. This means that in order to obtain an optimal amplification, the admittance parameters should be adjusted according to the actual robot configuration. In Labrecque and Gosselin [2015], a single variable that describes the manipulator's configuration for each Cartesian component is used to define a varying admittance control law. This variable is based on the Jacobian transformation, $\mathbf{J}$, in order to link the effect of Cartesian forces, $\delta\mathbf{f}$, on Cartesian

displacements, $\delta\mathbf{x}$, and yields

$$\delta\mathbf{x} = (\mathbf{J}\mathbf{K}_\theta{}^{-1}\mathbf{J}^T)\delta\mathbf{f}. \tag{3.21}$$

The matrix that includes all the Cartesian configuration-dependent variables is referred to as the Cartesian compliance matrix, noted $\mathbf{H}$, and is thus

$$\mathbf{H} = (\mathbf{J}\mathbf{K}_\theta{}^{-1}\mathbf{J}^T) \tag{3.22}$$

where $\mathbf{K}_\theta$ is the joint stiffness matrix. In this case, the joint stiffness matrix is diagonal and all joints are assumed to have the same stiffness, thus $\mathbf{K}_\theta = diag\{1,1,1,1,1,1\}$. Using the Cartesian compliance matrix as a configuration index, it thus becomes possible to optimize the controller parameters for all joint configurations, as explained in the following subsection.

3.4.2 Stability and performance

The stability of a bilateral amplification using admittance regulators for a Kuka LWR 4 has been demonstrated in Labrecque and Gosselin [2015] using a robust stability analysis. More specifically, the analysis makes use of the structured singular value (Packard and Doyle [1993]) with the human and environment dynamics as bounded uncertainties. This approach allows to define a stable parameter space for the pre-defined controllers used in the system — admittance controllers in this case — and a particular joint configuration.

Once this stability analysis is done, a cost function based on three performance indices is computed in the stable parameter space in order to assess the general performance of the controller. The three performance indices are :

1. the **amplification index**, also known as the kinematic correspondence index (Chang and Kim [2012]), which assesses the amplification capability of the system,
2. the **transparency index** based on the Z-width (Colgate and Brown [1994]), which evaluates the correspondence between the environment impedance and the impedance transmitted to the operator,
3. and the **integral of the time-weighted absolute error (ITAE) index**, which assesses the settling time and the overshoot of a transient response.

A performance cost is then associated to every set of controller variables contained in the stable parameter space. The set of variables with the smallest cost is thus selected as the optimal set for the joint configuration evaluated.

In the case of admittance controllers, three variables are included for each Cartesian regulator, namely, the virtual inertia m_v where $m_o = m_e = m_v$, the virtual damping c_v where $c_o = c_e = c_v$, and the amplification factor β_o or β_e. In order to ease the optimization process, it is possible to rearrange the three variables into only two parameters, for instance, the DC gain β_o/c_v and the time constant m_v/c_v.

With the Cartesian compliance variables of matrix (3.22), it thus becomes possible to define optimal control parameters for any manipulator configuration. Using this approach, a varying admittance control law is generated for the Kuka LWR 4 for bilateral amplification. An example of the resulting control law for 20 consecutive amplification configurations, i.e., compliances, for interactions with a stiff environment (stiffness between 4×10^5 and 2.6×10^5 N/m) is shown in Fig. 3.2. The time constant m_v/c_v is kept constant to its minimum value in order to respond as fast as possible, while the DC gain β_o/c_v varies proportionally with the compliance in order to ensure stable interactions. Indeed, the stiffer the environment, the more the gain is reduced. Most of the joint configuration compliances are found to be between 0.1 and 0.7, the varying gain is therefore bounded at these limit values. The environment DC gain β_e/c_v follows the same law but with a difference proportional to the amplification ratio.

During bilateral amplification, the Cartesian compliance matrix is thereby computed in real-time and preserves the optimal continuous gain scheduling law.

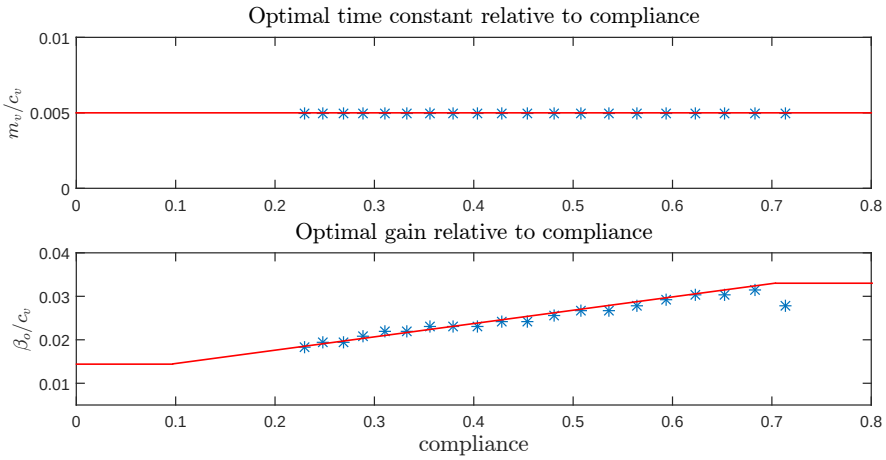

FIGURE 3.2 – Example of the gain scheduling law resulting from the optimization algorithm for bilateral amplification. The time constant m_v/c_v stays as low as possible and the DC gain β_o/c_v increases linearly with the compliance.

3.5 Transition

As explained in the previous sections, the admittance parameters have to be drastically different depending on the interaction mode. The main idea behind having the same control architecture for the two modes, namely, unilateral and bilateral, is to avoid the issues related to mode switching. Indeed, a recurrent issue for hybrid position/force control algorithms is the flickering effect that appears when the controller is switching between two states (Shaikh and Caines [2007]). Therefore, with a single adaptable controller, a smooth continuous transition can be implemented.

The transition control law consists simply in varying the current virtual inertia and damping

parameters to the desired virtual parameters. Therefore, in order to satisfy the unilateral and bilateral control laws, the admittance parameters are continuously computed for the two interaction modes depending on the manipulator's motion and configuration. Considering a single Cartesian degree of freedom, this transition law is applied when the external contact force between the robot and the environment, f_e, is contained between two selected limits noted f_{emin} and f_{emax}. The virtual damping is adjusted according to

$$c_{ov} = c_{uni} - \alpha_{amp}(|f_e| - f_{emax}) \tag{3.23}$$

where α_{amp} is defined as

$$\alpha_{amp} = \frac{c_{uni} - c_{bi}}{f_{emax} - f_{emin}} \tag{3.24}$$

in which c_{uni} and c_{bi} are the unilateral and bilateral virtual damping coefficients associated with the current manipulator motion and configuration. The virtual inertia is adjusted using

$$m_{ov} = \frac{m_o c_{ov}}{c_{uni}} e^{\gamma_{amp}(c_{ov} - c_{uni})} \tag{3.25}$$

where γ_{amp} is the smoothness parameter used to adjust the exponential transition, and yields

$$\gamma_{amp} = \frac{1}{c_{bi} - c_{uni}} \log\left(\frac{m_{bi} c_{uni}}{m_{uni} c_{bi}}\right) \tag{3.26}$$

where m_{uni} and m_{bi} are the current unilateral and bilateral virtual inertias associated with the current manipulator motion and configuration. An example is shown in Fig. 3.3 with $f_{emin} = 0$ N and $f_{emax} = 1$ N. The virtual damping changes from 20 to 50 Ns/m, and the virtual inertia changes from 4 to 0.19 kg.

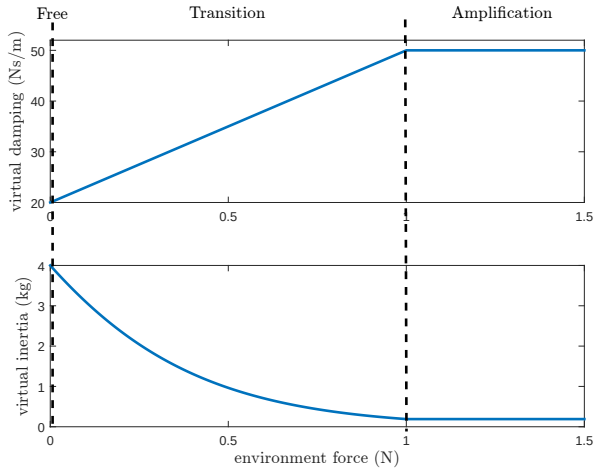

FIGURE 3.3 – Example of the effect of the transition law on the virtual damping and virtual inertia. The environment force is the contact force measured between the robot and the environment. The admittance parameters transit smoothly from the unilateral mode (free) to the bilateral mode (amplification).

This transition law generates an imperceptible switch between the two interaction modes without any flickering or sticking effect with the environment surface.

3.6 Experimentation

Three tests are presented here, which assess the stability and performance of the two control laws and their transition. The experimental setup includes a Kuka LWR 4, plus two six-axis ATI force/torque sensors, one mounted at the end-effector and the other one mounted on the fourth link of the manipulator with a handle, as shown in Fig. 3.4. The joint torque sensors were also used for the unilateral mode and an aluminium square tube was used as the rigid environment for the bilateral interaction. The parameter values for the different manipulator states are given in Table 3.1 and they satisfy the stability and performance requirements proposed in Sections 3.3, 3.4, and 3.5 for the specifications of the actual experimental setup.

TABLE 3.1 – Parameters for the experimentation.

parameter	value	parameter	value
β_o	1	β_k	0.5
c_o, c_k	20 Ns/m	β_e	0.2
m_o, m_k	4 kg	c_{bi}	30 to 70 Ns/m
α	2	m_{bi}	0.12 to 0.25 kg
η	0.1	compliance	0.1 to 0.7
γ	0.5	f_{emin}, f_{emax}	0 to 1 N

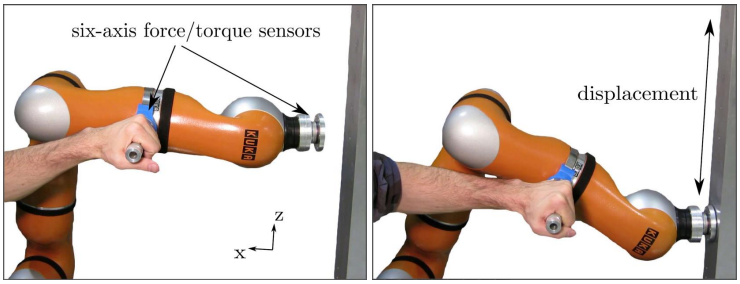

FIGURE 3.4 – Demonstration of the interaction interface with the Kuka LWR 4 (on the left) and of the horizontal amplification combined with a vertical displacement (on the right).

The first test aims at assessing the general stability and performance of the system. The task starts with a quick unilateral interaction, with the handle, in order to push the robot's end-effector against the rigid environment, which creates a strong impulse while the bilateral amplification mode is entered. The amplification is kept constant for a few seconds, and the end-effector is then pulled-off to go back to the unilateral mode. The interaction forces and the virtual damping measured while performing this task are shown in Fig. 3.5. It can be observed that the first unilateral interaction is an acceleration motion. The virtual damping is thus decreasing proportionally with the acceleration in order to ease the interaction — from 20 Ns/m down to 15.5 Ns/m — just before the end-effector hits the environment at around $t = 0.5$ second. Then, the system transits quickly to the bilateral mode with a virtual damping

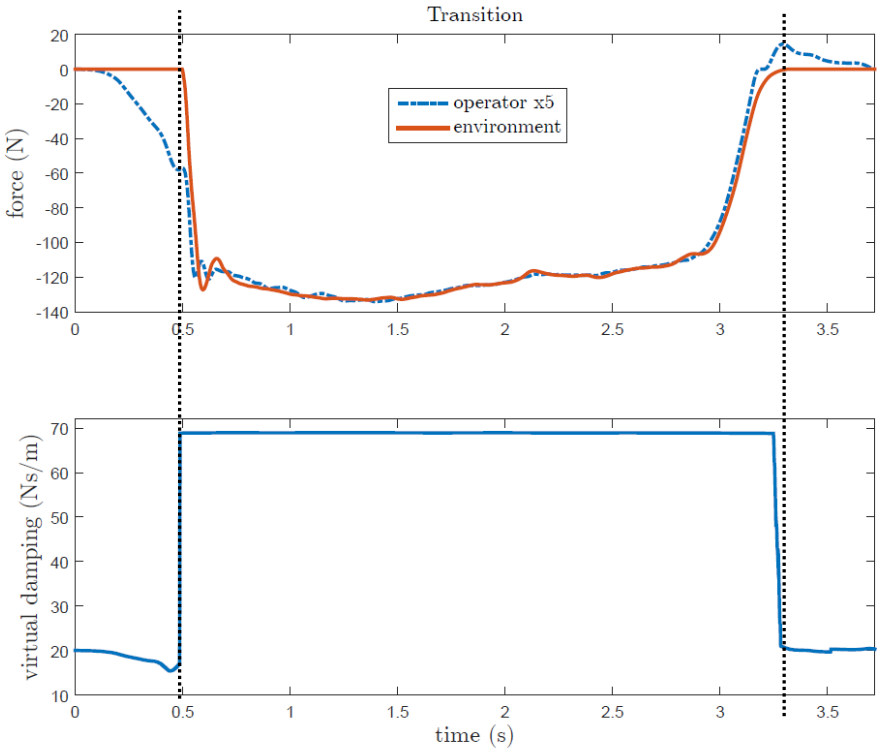

FIGURE 3.5 – Example of transition between the unilateral and bilateral interactions showing the general use of the system. The graphic of the virtual damping shows an example of the variation behaviour of the admittance parameters. The operator force is multiplied by 5 in order to provide a better visualization of the tracking quality.

around 69 Ns/m in order to reduce the overshoot and subsequently follow the commanded force — 5 times the operator force in this case. During the amplification, the end-effector is static and the operator attempts to keep a constant environment force of approximately 120 N. Small internal motions of the manipulator links slightly change the compliance, and thereby the virtual damping value — 0.1 Ns/m. However, this is imperceptible and not visible on the graph. The test ends with the pull-off at around $t = 3$ seconds where the action of the transition law is visible. Indeed, when the environment force reach -1 N at around $t = 3.25$ seconds the virtual damping is gradually decreased to the desired unilateral value. At the same time, this smooth mode transition generates the small operator force bump of 3 N. However, this force is too small and short in time to be felt by the operator and does not result into a sticking effect.

The second test aimed to evaluate the tracking performance for the velocity command. A test was conducted for each mode, namely, a vertical motion for the unilateral mode and a vertical displacement on the rigid aluminium surface for the bilateral mode, as depicted in Fig. 3.4. With these two tests, it was thus possible to compare the system's behaviour depending on the interaction. The tracking results are presented in Fig. 3.6. An interesting feature for the

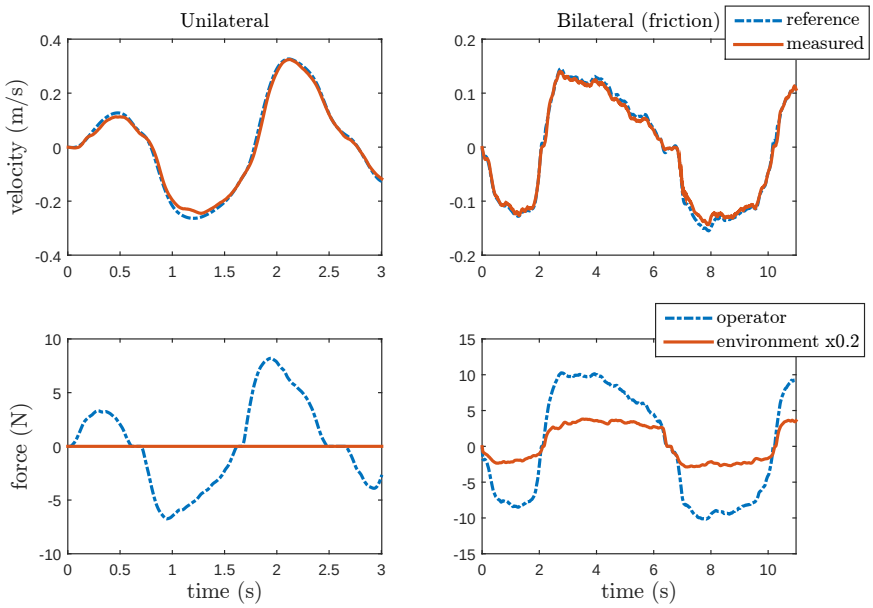

FIGURE 3.6 – Results of the velocity tracking test for the unilateral vertical motion (on the left) and for the bilateral vertical displacement on a rigid surface (on the right). The environment force is divided by 5 in order to obtain a visual comparison based on the applied operator force.

vertical displacement during the bilateral amplification — static 100 N environment force in the horizontal direction — is the presence of friction. Indeed, the friction force, which is proportional to the normal force applied on the environment, has to be overcome before generating an actual velocity command. In the test depicted in Fig. 3.6, the friction force is around 15 N. The operator thus needs to apply a force greater than 3 N to initiate the motion due to the amplification ratio of 5. Thereby, the resulting velocity command is based on the difference between the friction force and the operator force. The admittance parameters are therefore adjusted according to the bilateral control law (gain scheduling) and dictate the motion's dynamics. This approach leads to a highly responsive and stable interaction. In both cases, the unilateral and bilateral modes, the tracking performance between the measured and reference velocities are excellent. However, the unilateral motion is smoother, because of the high virtual inertia that has a greater impact on the filtering of the input force. The velocity command is also slightly delayed with the input force, while the bilateral velocity command rather coincides. This dynamics is desired for the unilateral mode and leads to the most intuitive interaction.

The last test aimed to assess the effect of the continuous gain scheduling law. A vertical displacement task with a horizontal bilateral amplification, as demonstrated in Fig. 3.4, was performed with and without the gain scheduling. The amplification factors are similar to those used in the previous experiments, i.e., the values reported in Table 3.1. The parameters for the gain scheduling case are also similar, but the admittance parameters for the constant case

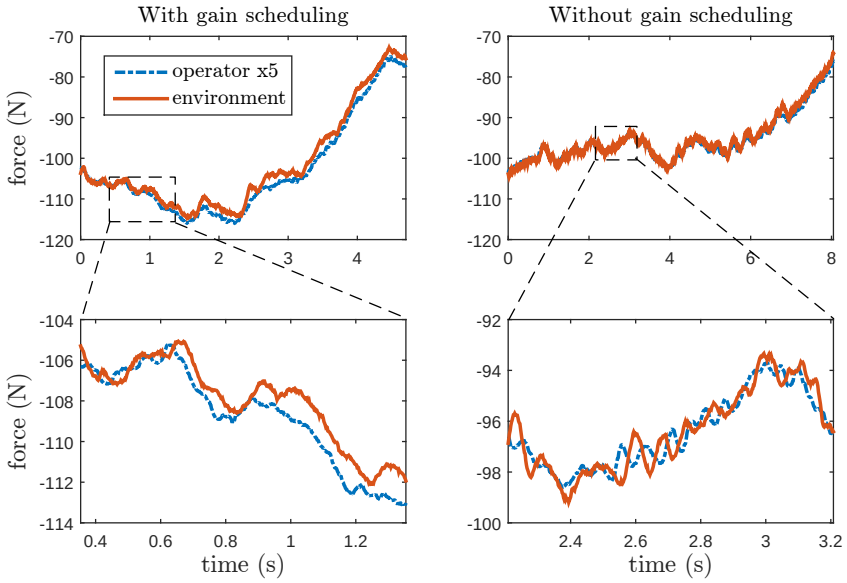

FIGURE 3.7 – Results of the force tracking for the horizontal amplification during the vertical displacement with gain scheduling (on the left) and with static parameter values (on the right). The operator force is multiplied by 5 in order to provide a better visualization of the tracking quality.

are set to $c_v = 0.12$ Ns/m and $m_v = 30$ kg. The results for a sample of the displacement are shown in Fig. 3.7. The amplification with constant parameters has in average a better tracking than the gain scheduling amplification. However, the gain scheduling interaction is definitively smoother than the one with constant parameters which, on the other hand, can be unstable for high impulses. It is also important to notice that the maximum error for the gain scheduling tracking in the cropped window of Fig. 3.7 is 1 N and reaches a maximum peak of 3 N for the full displacement. This peak error is small and demonstrates that the optimal gain scheduling law is not just leading to a high performance system but also to a robustly stable system.

In short, these three tests have demonstrated the potential to use admittance regulators for unilateral and bilateral interactions, even in the presence of a rigid environment.

3.7 Video Demonstration

The accompanying video demonstrates all situations to be addressed by the controller, namely, unilateral interaction, bilateral amplification and transition between both modes (*Chap3_Kuka_Uni_and_Bilateral.mp4*). The video also illustrates the stability and effectiveness of the gain scheduling control law using different configurations of the Kuka LWR 4 during bilateral interactions. Moreover, the force amplification is illustrated visually using the

displacement of a heavy payload. An example of a pHRI insertion task is also provided in the video. The video is available at

http://robot.gmc.ulaval.ca/publications/these-de-doctorat

3.8 Conclusion

In this chapter, a control architecture with variable admittance regulators for physical human-robot interaction was presented. The specific control laws detailed in this work adjust automatically to the interaction mode, namely, unilateral, transition, and bilateral, in order to provide the most intuitive and efficient interaction. Indeed, the unilateral variable control law aims at providing comfort and precision for the operator, while the bilateral gain scheduling is focused on stability and performance for the amplification, and whereas the transition control law ensures a smooth imperceptible transition from one mode to the other. The Kuka LWR 4 was used to demonstrate the effectiveness of the control architecture using three different experiments. A video extension of the chapter shows the intuitiveness of the resulting interaction. In conclusion, the use of a single controller structure such as the admittance controller is therefore viable for a highly effective and versatile pHRI. Future work includes the development of additional safety features since a human force enhancement device can be dangerous if not used properly.